Supporting Information

Vicente *et al.* 10.1073/pnas.0809353105

SI Materials and Methods

Models. For the first class of models investigated, we have simulated the dynamics of three reciprocally coupled single-compartment Hodgkin and Huxley (HH) neurons arranged as in the configuration shown in Fig. 1 of the main text. The temporal evolution of the voltage across the membrane of each neuron is given by

$$C\frac{dV}{dt} = -g_{Na}m^3h(V - E_{Na}) - g_K n^4(V - E_k) - g_L(V - E_L)$$
$$+ I_{ext} + I_{syn}, \qquad \text{[S1]}$$

where $C = 1$ μF/cm^2 is the membrane capacitance, the constants $g_{Na} = 120$ mS/cm^2, $g_K = 36$ mS/cm^2, and $g_L = 0.3$ mS/cm^2 are the maximal conductances of the sodium, potassium, and leakage channels, and $E_{Na} = 50$ mV, $E_K = -77$ mV, and $E_L = -54.5$ mV stand for the corresponding reversal potentials. According to HH formulation, the voltage-gated ion channels are described by the following set of differential equations

$$\frac{dm}{dt} = \alpha_m(V)(1 - m) - \beta_m(V)m, \qquad \text{[S2]}$$

$$\frac{dh}{dt} = \alpha_h(V)(1 - h) - \beta_h(V)h, \qquad \text{[S3]}$$

$$\frac{dn}{dt} = \alpha_n(V)(1 - n) - \beta_n(V)n, \qquad \text{[S4]}$$

where the gating variables $m(t)$, $h(t)$, and $n(t)$ represent the activation and inactivation of the sodium channels and the activation of the potassium channels, respectively. The experimentally fitted voltage-dependent transition rates are

$$\alpha_m(V) = \frac{0.1(V + 40)}{1 - \exp(-(V + 40)/10)}, \qquad \text{[S5]}$$

$$\beta_m(V) = 4\exp(-(V + 65)/18), \qquad \text{[S6]}$$

$$\alpha_h(V) = 0.07\exp(-(V + 65)/20), \qquad \text{[S7]}$$

$$\beta_h(V) = [1 + \exp(-(V + 35)/10)]^{-1}, \qquad \text{[S8]}$$

$$\alpha_n(V) = \frac{(V + 55)/10}{1 - \exp(-0.1(V + 55))}, \qquad \text{[S9]}$$

$$\beta_n(V) = 0.125\exp(-(V + 65)/80). \qquad \text{[S10]}$$

The synaptic transmission between neurons is modeled by a postsynaptic conductance change with the form of an α function

$$\alpha(t) = \frac{1}{\tau_d - \tau_r}(\exp(-t/\tau_d) - \exp(-t/\tau_r)), \qquad \text{[S11]}$$

where the parameters τ_d and τ_r stand for the decay and rise time of the function and determine the duration of the response. Synaptic rise and decay times were set to $\tau_r = 0.1$ and $\tau_d = 3$ ms, respectively, for the simulations exhibited in *Results* in the main text. Other sets of values running from 0.1 to 7 ms were also tested for such time constants. Finally, the synaptic current takes the form

$$I_{syn}(t) = -\frac{g_{max}}{N}\sum_{\tau_l}\sum_{spikes} \alpha(t - t_{spike} - \tau_l)(V(t) - E_{syn}), \qquad \text{[S12]}$$

where g_{max} (here fixed to 0.05 mS/cm^2) describes the maximal synaptic conductance, and the internal sum is extended over the train of presynaptic spikes occurring at t_{spike}. The delays arising from the finite conduction velocity of axons are taken into account through the latency time τ_l in the α function. Thus, the external sum covers the N different latencies that arise from the conduction velocities that different axons may have in connecting two neuronal populations. N was typically set to 500 in the simulations. For the single-latency case, all τ_l were set to the same value, whereas when studying the effect of a distribution of delays, we modeled such dispersion by a γ distribution with a probability density of

$$f(\tau_l) = \tau_l^{k-1}\frac{\exp(-\tau_l/\theta)}{\theta^k\Gamma(k)}, \qquad \text{[S13]}$$

where k and θ are shape and scale parameters of the γ distribution. The mean time delay is given by $\hat{\tau}_l = k\theta$.

Excitatory and inhibitory transmissions were differentiated by setting the synaptic reversal potential to be $E_{syn} = 0$ mV or $E_{syn} = -80$ mV, respectively. An external current stimulation I_{ext} was adjusted to a constant value of 10 μA/cm^2. Under such conditions, a single HH-type neuron enters into a periodic regime, firing action potentials at a natural period of $T_{nat} = 14.66$ ms.

The second class of models we have considered consists of three large balanced populations of integrate and fire (IAF) neurons. Each population was composed of 4,175 IAF neurons from which $\approx 80\%$ were excitatory. The local connectivity was sparse and random. Each neuron received thus a synapse from 10% of randomly selected cells inside its population and from 0.25% from the excitatory class of the neighboring populations. The voltage dynamics of each neuron was then given by the following equation

$$\tau_m\frac{dV_i}{dt} = -V_i(t) + RI_i(t), \qquad \text{[S14]}$$

where τ_m stands for the membrane constant and $I(t)$ is a term collecting the currents arriving to the soma. The latter is decomposed in postsynaptic currents and external Poissonian noise

$$RI_i(t) = \tau_m\sum_j J_j\sum_k \delta(t - t_j^k - \tau_l) + A\xi_i, \qquad \text{[S15]}$$

where J_j is the postsynaptic potential amplitude, t_j^k is the emission time of the kth spike at neuron j, and τ_l is the transmission axonal delay. The external noise ζ_i is simulated by subjecting each neuron to the simultaneous input of 1,000 independent homogeneous Poissonian action potential trains with an individual rate of 5 Hz. Different cells were subjected to different realizations of the Poissonian processes to ensure the independence of noise sources for each neuron. J_{exc} and A amplitudes were set to 0.1 mV. The balance of the network was controlled by setting $J_{inh} = -gJ_{exc}$, with g ranging from 3.5 to 4 to compensate the outnumbering of excitatory units.

The dynamics of each neuron evolved from the reset potential of $V_r = 10$ mV by means of the synaptic currents up to the time when the potential of the ith neurons reached a threshold of 20 mV, a value at which the neuron fires and its potential relaxes to V_r. The

potential is clamped then to this quantity for a refractory period of 2 ms during which no event can perturb this neuron.

Simulations. The set of Eq. **S1–S12** was numerically integrated using the Heun method with a time step of 0.02 ms. For the first class of models we investigated, i.e., the three HH cells neuronal circuit, we proceeded as follows. Starting from random initial conditions, each neuron was first simulated without any synaptic coupling for 200 ms, after which frequency adaptation occurred, and each neuron settled into a periodic firing regime with a well-defined frequency. The relation between the phases of the oscillatory activities of the neurons at the end of this warm-up time was entirely determined by the initial conditions. After this period and once the synaptic transmission was activated, a simulation time of 3 s was recorded. This allowed us to trace the change in the relative timing of the spikes induced by the synaptic coupling in this neural circuit.

The second class of model involving the interaction of heterogeneous large populations of neurons was built with the neuronal simulator package NEST (1). The simulation of such networks uses a precise time-driven algorithm with the characteristic that the spike events are not constrained to the discrete time lattice. In a first stage of the simulation the three populations were initialized being isolated from each other and let them to evolve just due to their internal local connectivity and external Poissonian noise. In a subsequent phase, the three populations were interconnected according to the motif investigated here and simulated during 1 s.

Data Analysis. The strength of the synchronization and the phase difference between each individual pair of neurons (m, n) were derived for the first model of three HH neurons by the computation of the order parameter defined as

$$\rho(t) = \frac{1}{2} \left| \exp(i\phi_m(t)) + \exp(i\phi_n(t)) \right|, \qquad \textbf{[S16]}$$

which takes the value of 1 when two systems oscillate in-phase and 0 when they oscillate in an antiphase regime or in an uncorrelated fashion. To compute this quantifier, it is only necessary to estimate the phases of the individual neural oscillators. An advantage of this method is that one can easily reconstruct the phase of a neuronal oscillation from the train of spikes without the need of recording the full membrane potential time series (2). The idea behind this is that the time interval between two well-defined events (such as action potentials) defines a complete cycle, and the phase increase during this time amounts to 2π. Then, linear interpolation is used to assign a value to the phase between the spike events.

The synchrony among the large populations of neurons of the second model studied in the article was assessed by the computation of averaged cross-correlograms. For that purpose, we randomly selected three neurons (one from each of the three populations) and computed for each pair of neurons belonging to different populations the histogram of coincidences (bin size of 2 ms) as a function of the time shift of one of the spike trains. We computed the cross-correlograms within the time window ranging from 500 to 1,000 ms to avoid the transients toward the synchronous state. The procedure was repeated 300 times to give rise to the estimated averaged distributions of coincidences exhibited in Figs. 5 and 6 in the main text.

Stability Computations. In this section, we follow an analytical approach to compute the stability of the zero lag synchronization of outer neurons interacting through a dynamical relaying element (see the motif shown in Fig. 1 *Top* in the main text). In particular, we demonstrate that the stability of such solution extends over larger regions of the axonal delay parameter than

for the case of only two neurons interacting directly. These calculations are performed under the phase reduction approximation of the spiking dynamics of neurons, which assume that the oscillatory activity of each neuron can be described by a phase variable.

The dynamics of each cell in the motif is then described as

$$\frac{d\theta_i}{dt} = \frac{1}{T_i} + \sum_{n,k} a_{i,k} \delta(t - t_k^n - \tau)\Delta(\theta_i), \qquad \textbf{[S17]}$$

where θ_i is the phase of each neuron within its spiking cycle, T_i amounts to the natural period, $a_{i,k}$ is the strength of the interaction between neurons, and t_k^n represents the time of the nth spike of the kth neuron (3). The axonal delay in the communication between the neurons is taken into account by the temporal latency τ. The pulse-coupled interaction among the neurons is captured by the phase response curve (PRC) $\Delta(\theta)$. This curve characterizes the change in the cycle period (phase shift) of an oscillator induced by a perturbation as a function of the timing at which it is received. It is defined as

$$\Delta(\theta) \equiv 1 - \frac{T^*(\theta)}{T}, \qquad \textbf{[S18]}$$

where T^* is the new period of the oscillation induced by a perturbation injected at the phase θ. PRCs of neurons and many other biological oscillators have been measured experimentally as well as computed for models and provide a rigorous framework to predict the dynamical properties of spiking neurons (4, 5). A recent example of the use of the PRC method in small networks of biological neurons can also be found in ref. 6.

Once we establish the basic equations for the pulse-coupled interaction among neurons, we proceed by computing the possible phase locked states. Before that step we change first the reference system of our phase variables by defining the new phase φ such that $\theta \equiv vt + \varphi(t)$, with $v = 1/T$. Assuming identical natural periods of the cells ($v_1 = v_2 = v_3 = v$), Eq. **S17** is rewritten for the motif of three neurons interacting through dynamical relaying as

$$\frac{d\varphi_1}{dt} = a_{1,2}\sum_n \delta(t - t_2^n - \tau)\Delta(vt + \varphi_1),$$

$$\frac{d\varphi_2}{dt} = a_{2,1}\sum_n \delta(t - t_1^n - \tau)\Delta(vt + \varphi_2)$$

$$+ a_{2,3}\sum_n \delta(t - t_3^n - \tau)\Delta(vt + \varphi_2),$$

$$\frac{d\varphi_3}{dt} = a_{3,2}\sum_n \delta(t - t_2^n - \tau)\Delta(vt + \varphi_3). \qquad \textbf{[S19]}$$

Following ref. 3 in the weak coupling case, one can approximate the nth spiking time of each neuron as $t_i^n \approx \frac{n - \varphi_i}{v}$. Substituting this expression in Eq. **S19** and averaging the instantaneous coupling over a full period of the oscillation results in

$$\frac{d\varphi_1}{dt} = a_{1,2}\Delta(\varphi_1 - \varphi_2 + v\tau),$$

$$\frac{d\varphi_2}{dt} = a_{2,1}\Delta(\varphi_2 - \varphi_1 + v\tau) + a_{2,3}\Delta(\varphi_2 - \varphi_3 + v\tau),$$

$$\frac{d\varphi_3}{dt} = a_{3,2}\Delta(\varphi_3 - \varphi_2 + v\tau). \qquad \textbf{[S20]}$$

Phase-locked solutions take the form $\varphi_i(t) = \Omega t + \phi_i$, with ϕ_i being a constant. The existence of the zero phase lag solution between the outer neurons ($\phi_1 = \phi_3$) requires the following conditions being satisfied simultaneously

$$a_{1,2} = a_{3,2},$$

$$(a_{2,1} + a_{2,3})\Delta(\phi_2 - \phi_1 + v\tau) = a_{1,2}\Delta(\phi_1 - \phi_2 + v\tau). \quad \textbf{[S21]}$$

For simplicity, we consider the case where synaptic strength is normalized by the number of afferent inputs of each neuron so that the total coupling strength per neuron is the same ($a_{2,1} + a_{2,3} = a_{1,2} \equiv a$). In such case, the second condition is simply $\Delta(\phi_2 - \phi_1 + v\tau) = \Delta(\phi_1 - \phi_2 + v\tau)$. This condition can have multiple solutions depending on the specific PRC of the neuron class that we are interested in. In any case, two important solutions that hold for any PRC are $\phi_1 - \phi_2 = 0$ and $\phi_1 - \phi_2 = 1/2$. These solutions are the in-phase and antiphase relations for nearest neighbors oscillators.

A linear stability analysis for perturbations of the phase-locked solutions ($\varphi_i = \Omega t + \phi_i + \delta\phi_i$) gives rises to the system

$$\frac{d\delta\phi_1}{dt} = a\Delta'(\phi_1 - \phi_2 + v\tau)(\delta\phi_1 - \delta\phi_2),$$

$$\frac{d\delta\phi_2}{dt} = \frac{a}{2}\Delta'(\phi_2 - \phi_1 + v\tau)(2\delta\phi_2 - \delta\phi_1 - \delta\phi_3),$$

$$\frac{d\delta\phi_3}{dt} = a\Delta'(\phi_1 - \phi_2 + v\tau)(\delta\phi_3 - \delta\phi_2), \quad \textbf{[S22]}$$

where $'$ stands for the derivative operator. The eigenvalues of the characteristic equation are $\lambda_1 = a[\Delta'(\phi_1 - \phi_2 + v\tau) + \Delta'(\phi_2 - \phi_1 + v\tau)]$, $\lambda_2 = 0$, and $\lambda_3 = a\Delta'(\phi_1 - \phi_2 + v\tau)$ for the corresponding eigenvectors $\bar{V}_1 = [1, -\Delta'(\varphi_2 - \varphi_1 + v\tau)/\Delta'(\varphi_1 -$

$\varphi_2 + v\tau), 1]$, $\bar{V}_2 = (1,1,1)$, and $\bar{V}_3 = (-1,0,1)$. For the in-phase and antiphase nearest-neighbors relations, the stability condition of the negativity of the eigenvalues reduces to the cases of $a\Delta'(v\tau) < 0$ and $a\Delta'(1/2 + v\tau) < 0$, respectively. The main role of the delay in this simplified description of the neuronal dynamics is to shift the phase at which a neuron receives the perturbation from the other neurons, which can substantially modify the stability of the solutions.

It is important to notice that for two directly coupled neurons, the zero phase lag synchronization exclusively corresponds to the in-phase nearest-neighbor relation. However, for the case of three neurons interacting as arranged in a bidirectional chain, both the nearest-neighbor in-phase and antiphase relations result in a zero phase solution for the outer neurons in the motif. This allows the outer neurons to fire isochronously for such delays where any of the two nearest-neighbor phase relations are stable and thus increases the delay range over which zero phase synchrony can appear. The precise range of stability must be computed specifically for each type of PRC according to the former stability criterion, but a general result is that such range is larger for the network motif under study than for the direct coupling of two neurons. In fact, when computing the phase relation for nearest neighbors in the full HH model of three neurons interacting through dynamical relaying, we could observe how this relation strongly varies as a function of the axonal delay (see Fig. S1). For some delays, the nearest-neighbor neurons were in-phase, but varying the delay they were observed to enter into states in which the antiphase solution dominated. For only two directly coupled neurons such changes limited the range of delays for which they could synchronize without any lag. However, the phase relation between the outer neurons 1 and 3 in the relaying motif was unsensitive to such sudden changes in the nearest-neighbor phase relation and remained in a zero lag solution for almost all explored delays up to 30 ms.

1. Brette R, et al. (2007) Simulation of networks of spiking neurons: A review of tools and strategies. J Comp Neurosci 23:349–398.
2. Pikovsky A, Rosemblum M, Kurths J (2002) Synchronization: A Universal Concept in Nonlinear Science (Cambridge Univ Press, Cambridge, UK).
3. Goel P, Ermentrout B (2002) Synchrony, stability, and firing patterns in pulse-coupled oscillators. Physica D 163:191–216.
4. Hansel D, Mato G, Meunier C (1995) Synchrony in excitatory neural networks. Neural Net 7:307–337.
5. Galan R, Ermentrout GB, Urban NN (2005) Efficient estimation of phase-resetting curves in real neurons and its significance for neural-network modeling. Phys Rev Lett 94:158101.
6. Pervouchine DD, et al. (2006) Low dimensional maps encoding dynamics in the entorhinal cortex and hippocampus. Neural Comp 18:2617–2750.
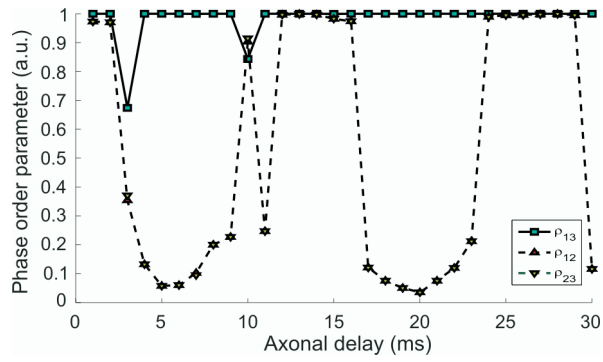
Fig. S1. Synchronization index at zero lag for pairs of HH neurons 1 and 3 (squares), 1 and 2 (upright triangles), and 2 and 3 (inverted triangles) as a function of the axonal delay. The coupling is excitatory, and the neurons are interacting according to the scheme in Fig. 1 *Top* in the main text. The sudden decays of the synchronization index between nearest neighbor neurons usually indicate the transitions to antiphase states. Notice that the zero-phase relation between neurons 1 and 3 is almost insensitive to such changes.